Analyst

Accepted Manuscript

ROYAL SOCIETY OF CHEMISTRY

www.rsc.org/analyst

Journal Name

RSCPublishing

ARTICLE

Multiplex single particle analysis in microfluidics

Cite this: DOI: 10.1039/x0xx00000x

D. Dannhauser,[ab*] G. Romeo,[ab†] F. Causa,[abc] I. De Santo[ab] and P. A. Netti[abc]

Received 00th January 2012,
Accepted 00th January 2012

DOI: 10.1039/x0xx00000x

www.rsc.org/

A straightforward way to measure separated micrometric sized particles in microfluidic flow is reported. The light scattering profile (LSP) of each single particle is fully characterized by a CMOS-camera based small angle light scattering (SALS) apparatus, ranging from 2° up to 30°. To ensure controlled particle passing through the incident laser, a viscoelastic 3D alignment effect by viscoelastic induced particle migration has been implemented in a simple and cost-effective microfluidic device. Different polystyrene particle sizes are measured in microfluidic flows and the obtained scattering signatures are matched with a Lorenz-Mie based scattering theory. The results confirm the possibility to use this apparatus for real multiplex particle analyses in microfluidic particle flows.

Introduction

The characterization of micrometric particles from scattering patterns obtained by light interaction is a well known technique used in several areas of research as well as in industrial applications. The achieved light scattering profile (LSP) over a wide angular range provides a fast and accurate measurement of morphological particle properties (refractive index, size, shape, etc), resulting in a sensitive tool for discriminating between different cell types or between healthy and malignant cells, or to probe changes in cells resulting from stimuli.[1]

The LSP works like a unique scattering signature; generally, such signatures are obtained by particle suspension measurements, which can be divided into static light scattering (SLS)[2,3], dynamic light scattering (DLS)[4,5] and SLS+DLS[6]. In modern microfluidic applications, detailed analyses of individual multiplex particle properties are highly desirable. Flow-cytometry based systems[7], where single particles flowing one at a time through a small illuminated aperture, generally collect the scattering intensity at a few fixed scattering angles θ. A more complex cytometer system is the scanning flow cytometer (SFC)[8], which allows the individual particle measurement over a wide LSP range -up to 500 particles/s- using the flying light scattering indicatrix method[9]. SFC measures single particles over time by diverse PMTs, instead of the collection of a continuous LSP at a single moment with a multi-element sensor using a pixel array of a CCD or CMOS-camera sensor. The use of a camera significantly simplifies the LSP measurement and overall complexity of individual particle measurement systems. Another technique, the holographic video microscopy approach[10,11] measures very precisely size and refractive index of individual particles. Though very accurate, this approach needs high numerical aperture objectives and thorough data analysis.

For the analyses of a single micrometer sized particle -spanning from 1 up 10 μm- in microfluidic flows it appears that the small angle light scattering (SALS) range is a promising approach. The distinct LSPs at SALS measurements can be used to precisely reconstruct the morphological features of an unknown particle.

Nevertheless, individual particle measurements require an accurate 3D particle alignment according to the incident laser beam. It has recently been shown that viscoelastic induced particle migration in a round shaped capillary can be used to obtain precise 3D particle alignment in microfluidic flows.[12] This simple alignment technique -combined with the possibility to use particle or cell specific physiological fluids and an adjustable particle velocity range- makes this approach interesting for biological individual cell measurements. The combination of a SALS measurement system over a wide continuous LSP and the viscoelastic based particle alignment opens up the possibility for precise characterization of unknown morphological features of an individual particle without changing its physiological medium.

In order to measure separated particles of micrometric size, a laser beam has to be bundled in a narrow size range smaller than a few hundred of microns in diameter to illuminate micrometric particle one at a time in microfluidic flow. A consistent particle alignment according to the incident laser beam position, with minimized light interaction from the measuring chamber itself or the incident beamstop, represents the critical issue in the implementation of SALS as a detection tool.

In this work we present a SALS apparatus -whose concept had been previously sketched-[13] able to accurately analyse the LSPs of different single particles in microfluidic flows. A continuous LSP detection spanning from $2° < \theta < 30°$ has been achieved thanks to a narrow incident beam collimation and an optimized

scattered light collection system. To our knowledge, no other SLS apparatus in literature combines such a wide scattering range with the possibility of individual particle characterization in microfluidic flows. Multiplex particle sizes are measured in a rectangular shaped chamber combined with a viscoelastic particle alignment part, obtained by viscoelastic induced particle migration. This simple combination of exact particle alignment and observation area in a single low-cost device opens the possibility of precise single particle analyses in microfluidic flows. Indeed, by matching the experimental LSP of a particle to that predicted by theory, it is possible to obtain simultaneously particle size and refractive index of the measured unknown particles in a cost-effective system.

Experimental Setup

Optical setup

Our apparatus measures individual micrometric sized particles at different forward angles in-flow condition; in Fig. 1 the apparatus is schematically illustrated. The distinguishing advantage of this setup compared to systems known in literature[2-7], is its simplicity for the in-flow measurement of a micrometric particle over a continuous LSP of $2° < \theta < 30°$.

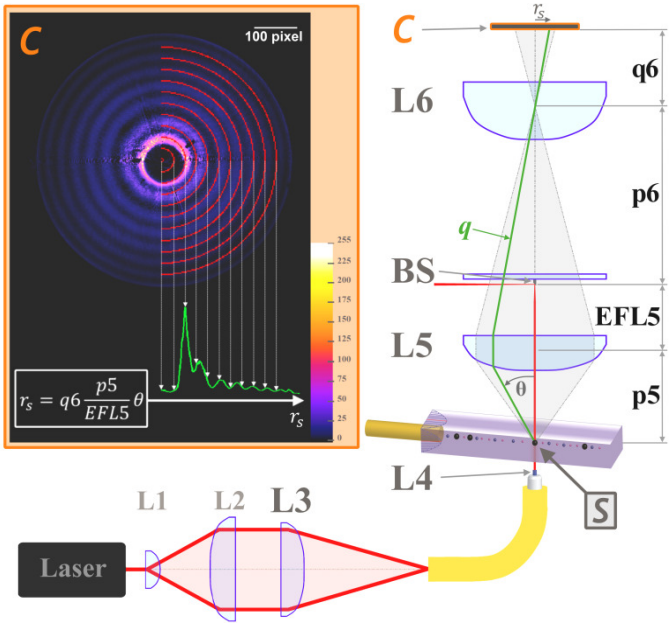

Fig 1. Schematic diagram of the apparatus. L1 & L2 expand the laser beam, while L3 focuses the laser light in the optical fibre. L4 indicates the collimation lens at the end of the optical fibre, while S indicates the position of the target particle in the microfluidic device. The lenses L5 & L6 collect and map the scattered light on the camera sensor C. BS shows the beamstop, reflecting the incident light out of the system. In inset C, the scattering pattern measured after background subtraction is overlaid with a demonstrative number of red rings each corresponding to a certain pixel radius value. The green curve shows the obtained LSP over the whole measured q-range.

The used light source is a 5 mW linear polarized HeNe laser, operating at a wavelength $\lambda = 632.8\,nm$. The laser output is directly aligned into a beam expander ($L1$, $L2$) that enlarges the beam waist 20 times. Two mirrors in series (not shown), adjust the laser light direction and an achromatic lens ($L3$) with a focal length of 125 mm focuses the laser in the entrance of a single mode fibre.

To obtain a small and quasi-collimated laser beam size at the target sample region S, a gradient-index (GRIN) lens ($L4$) with a working distance equal to zero is glued to the exit of the optical fibre. This procedure results in a beam diameter of $2 \times \omega_0[1 + (\lambda z/\pi\omega_0{}^2)^2]^{1/2} = 108.37 \approx 110\ \mu m$ at the measurement position S, where $z = 1.2\,mm$ is the distance between $L4$ and S. The beam waist ω_0 exiting the optical fibre is calculated by $\omega_0 = NA \cdot f = 0.12 \cdot 450\ \mu m = 54\ \mu m$, where NA is the numerical aperture of the fibre and f the focal length of L4. The expected laser divergence is calculated as $2 \times (\lambda/\pi\omega_0) = 7.46\,mrad$. Such small divergence combined with a beam diameter of around 110 μm enables a precise individual particle analysis.

To ensure that particles are vertically and horizontally aligned along the central axis while passing the laser beam, a specific microfluidic device was designed using a simple and cost-effective microfluidic alignment technique. The device is placed on a XY- and Z-stage for accurate positioning of the flowing particle axis according to the incident beam centre.

An aspheric lens ($L5$) with high numerical aperture ($NA = 0.83$) and optical magnification of 8.54, collects the emitted forward scattering of each particle passing through the laser beam. The limitation of the measureable scattering angle is mainly due to the numerical aperture and the absolute distance $p5 = 16.86\,mm$ from $L5$ to S. Moreover, the beamstop size of 1 mm (BS), which is placed at the back-focal plane of $L5$ ($EFL5 = 15.09\,mm$) and the clear aperture of $L5$ further restrict the measurable scattering range, giving a theoretical LSP of $1.9° < \theta < 33.7°$ for this system. At the end of the LSP collection system, a plano-convex lens ($L6$) with magnification $M_6 = 0.24556$ and distance $p6 = (p5 \cdot EFL5/p5 - EFL5) - EFL5 = 129\,mm$ after the BS, maps the scattered light on the CMOS-camera sensor (C - HAMAMATSU PHOTONICS – C11440-22CU). The camera has a pixel size of 6.5 μm and is placed at a distance $q6 = (p6 \cdot EFL6)/(p6 - EFL6) = 31.68\,mm$ after $L6$. The afore-mentioned LSP collection system is designed to obtain far-field images at a short distance of $p5 + EFL5 + p6 + q6 = 192.63\,mm$.

By knowing all optical distances, it becomes then possible to calculate the LSP over the measureable scattering range.

Viscoelastic particle alignment setup

In-flow measurements are accomplished in a microfluidic system (Fig. 2) composed by a particle alignment section and a particle measuring section.

The viscoelastic particle alignment is achieved in a round shaped capillary where, thanks to a viscoelastic suspending fluid, particles migrate towards the channel central axis, as already demonstrated in a previous work from our group.[12] The particle aligning capillary enters a rectangular shaped measuring chamber from the side, resulting in a coincident central axis. The obtained 3D aligned particle stream is kept along the central axis flowing through the measuring chamber

thus allowing the laser beam to efficiently interrogate the particles one at a time at the measurement position S (see detailed in Fig. 2). No specific distance between the capillary output and the end of the measuring chamber is prescribed for S. A distance of $\sim 15\ mm$ after the capillary exit was chosen for the experimental measurements.

Due to the presence of normal stress differences, it is well-known that viscoelastic liquids induce particle migration in a certain range of shear rates.[12] The above-mentioned phenomena results in effective 3D particle alignment under the following condition of $\Theta \approx \dot{\gamma}\,\lambda_t + \beta^2\, L/r_c > 1$, as already demonstrated in a previous work.[14] This implies a certain shear rate $\dot{\gamma} = (\Delta P\, r_c)\,/\,(8\,\eta\, L)$, as well as given rheological relaxation time λ_t and viscosity η, together with a proper minimum capillary length L for optimal 3D particle alignment fulfilment. Note that the blockage ratio $\beta = a/r_c$, with particle radius a and inner capillary radius r_c, is necessary to stay in a certain range of 0.038– 0.160.

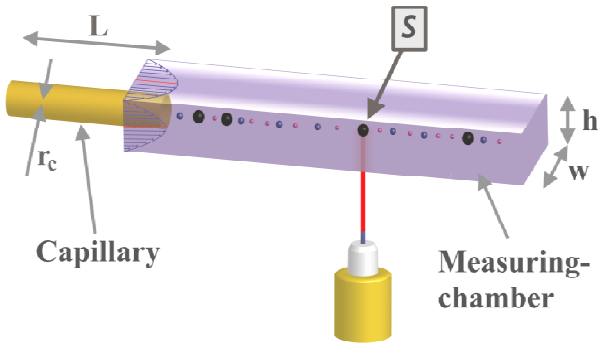

Fig. 2 Schematic illustration of the 3D particle alignment. A round glass capillary enters the measuring chamber from the side, providing 3D particles alignment along the central axis. A minimum capillary length L combined with given inner radius of the capillary r_c allow precise particle alignment. S indicates the measurement position of the apparatus, while h and w indicate height and width of the chamber, respectively. The ferrule connecting the capillary to the chamber is not shown for readability.

To accomplish the precise particle alignment, a viscoelastic liquid consisting of 0.4% polyethylene oxide (PEO $M_w = 4\ MDA$) by weight was used. Rheological liquid parameters like zero-shear viscosity $\eta = 0.013\ Pa\ s$ and relaxation time $\lambda_t = 0.1\ ms$ were obtained by plate-plate configured Rheometer measurements. (data not shown). A capillary with $r_c = 25\ \mu m$ and $L = 50\ cm$ and adjusted $\Delta P = 500\ mbar$ connected to the microfluidic device, together with the rheological features of the used PEO solution ensure the correct operating conditions for the viscoelastic particle alignment.

Materials and Methods

Materials

The functionality of the apparatus was tested with polystyrene latex (PSL) particles (POLYSCIENCE* & SIGMA-ALDRICH) of different sizes, spanning from 0.947 up to 4.010 μm (reported in Table 1). All measurements were carried out with strongly diluted particle solutions, reducing multi-particle scattering effects. For quiescent measurements, rectangular glass microslides with a chamber size of w: 4000 μm and h: 200 μm were placed at the target particle plane.

In-flow measurements were carried out with our *ad hoc* designed microfluidic device. The whole microfluidic alignment system consists of only 4 single parts: a round glass capillary, a pressure pump, a measuring chamber and a soft ferrule, resulting in a simple and cost effective system easy to implement in diverse light scattering systems. The measuring chamber is made out of two separate high quality PMMA parts. Both parts were machined *via* micromilling and clamped together with ethanol and temperature (65 °C) over 24 hours to create a unique measuring chamber. (see Fig. 3). A round capillary with inner radius $r_c = 25\ \mu m$ enters the measuring chamber (*w:* 381 μm, *h:* 400 μm) from the side through a soft ferrule, which seals the chamber entrance. The measuring chamber is 40 mm long and enlarges after its mid-point to a width of 508 μm, resulting in two different measuring velocities in one device. A reservoir at the end of the chamber collects all measured liquids.

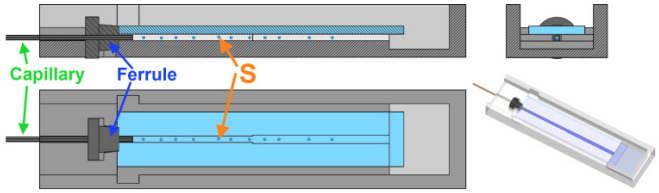

Fig. 3 Front, top and side view of the microfluidic device. The PMMA cover slide is illustrated in light blue, while S indicates the particle measurement position. The ferrule holds the capillary in place and seals the measuring chamber.

Methods

A – Scattering calculation

Generally, each light speckle collected by the camera corresponds to the same magnitude of the scattering wave-vector $q \equiv |q|$, but with different azimuthal orientations, and is collected in a single scattering ring $r_s = q6(p5/EFL5)\theta$ (indicated by a mask of demonstrative red rings in the inset of Fig. 1). The average intensity of these rings is plotted over the q-range of the camera (indicated as green LSP), where the acquired LSP is generally defined as $q = 4\pi\lambda^{-1} m_m \sin(\theta/2)$, with $\theta = r_s/(EFL5 \cdot M_6)$ corresponding to the pixel ring radius and m_m to the refractive index of the ambient medium.

Quiescent and in-flow measured LSPs of individual particles were compared to calculations based on the Lorenz-Mie theory by a Matlab routine. The general particle scattering coefficient and amplitude calculations are based on the un-polarized Lorenz-Mie solution[15]. The intensity pattern scattered by a particle (scattering signature) is described by $I_s(\theta) = I_0(|S_1|^2 + |S_2|^2)/2k^2r^2$ where r is the particle to detector distance, I_0 the incident light intensity, and k the wave-number. The scattering amplitudes are defined as $S_1(\cos\theta) = \sum_{n=1}^{\infty}[2n+1/n(n+1)]\,(a_n\pi_n + b_n\tau_n)$ and $S_2(\cos\theta) = \sum_{n=1}^{\infty}[2n+1/n(n+1)]\,(a_n\tau_n + b_n\pi_n)$ with the scattering coefficients a_n and b_n of the scattering field, where n is the expansion index going from $n = 1$ to $\rightarrow \infty$.[16]

The interaction of incident light with a sphere causes radiation of electromagnetic waves, which are generally not isotropic. The use of vector spherical harmonics opens the possibility to expand the incident, scattered and internal field of a homogeneous sphere. These expansion coefficients a_n and b_n, are generally expressed with the magnetic permeability of the medium and that of the sphere. The functions $\pi_n(\theta)$ and $\tau_n(\theta)$ describe the angular LSP of the spherical harmonics, while the size parameter $x = 2\pi Na/\lambda$ and the relative refractive index $m = m_p/m_m$ of the scattering coefficients are given with a the radius of a sphere, and m_p and m_m the refractive indices of particle and ambient medium, respectively. The correlation between the measured LSP and predictions from $I_s(\theta)$ makes it possible to obtain simultaneously particle size and refractive index.

The real (dispersive) part of the refractive index is given as $m_p = 1.58722$ for PSL particles, whereas the PEO solution can be assumed to be equal to H_2O with $m_m = 1.3317$.[17,18]

B – Acquisition

For each in-flow measurement, 4000 frames with a frame rate of 20 fps are collected. The image containing the LSP of a particle is determined as the frame with the highest mean intensity related to previous measured frames (see Fig. 4a). Once the frame with the highest intensity is determined, the average intensity of each individual pixel over 3 successive frames centring the determined one is calculated, reducing thermal noise effects of the sensor and the incident laser beam fluctuations (Fig. 4b).

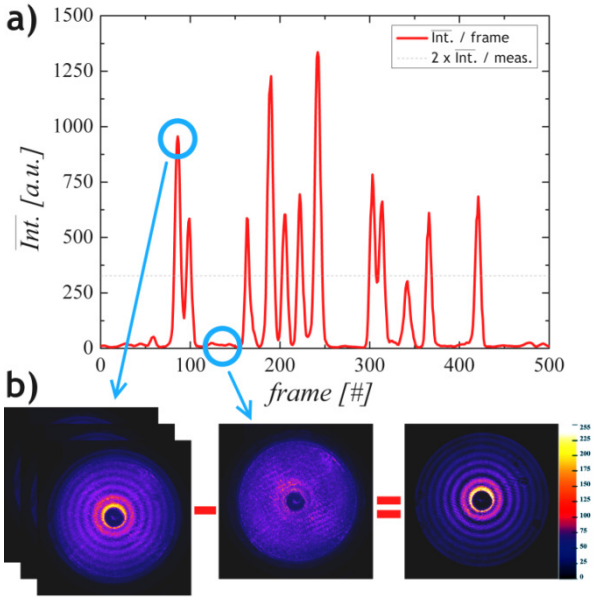

Fig. 4 a) The mean Intensity of each single frame for a part of a in-flow measurement is plotted. The dashed line indicates the threshold value (2 x overall mean intensity) for particle analyses. b) The average intensity of each pixel over 3 successive frames centring the detected frame is calculated. The background light intensity is subtracted from the averaged frame, resulting in the final particle frame.

Note that in view of the relatively high frame rate compared to the low particle velocity in the microfluidic device, no significant LSP change over 3 successive frames can be recognized. This implies that the data reduction procedure does not affect the morphological information of a particle. On the other hand, for quiescent particle measurements, once a particle is detected each pixel is averaged over 100 successive frames to obtain the averaged intensity frame.

The background light intensity of each measurement is averaged over 50 successive frames of the pure medium filled devices, to correct for transmission and LSP collection system influences. For each individual particle the background signal is subtracted and the LSP is calculated.

Growing pixel-rings with the width of one pixel starting from $r_s = 1$ up to a radius value of 400 pixels are used to average the q-value at each pixel distance. Note that each ring of pixels is averaged over the amount of pixels in the ring. The resulting values show the LSP of a particle according to the pixel size of the camera. For optimal particle analysis, the used LSP is limited to a q-range from 0.5 μm^{-1} up to 6.8 μm^{-1}, reducing possible optical aberration or vignetting effects. However, the particle radius of the measured particle is established by overlaying with the best matching Lorenz-Mie LSP.

By pre-calculation of such LSP curves -in a meaningful size and refractive index range- a comparison-table can be created and used for online comparison of the measured LSPs to the best matching theory.

C – Calibration

For a precise adjustment of the apparatus, far-field patterns from differently sized pinholes are compared to the Fraunhofer diffraction theory for a circular aperture[19]. The pinhole position is chosen exactly at the particle position S. The alignment is achieved through the analysis of LSPs (Fig. 5) from the pinholes.

We are able to distinguish the Airy patterns predicted by theory up to $q \approx 5\mu m^{-1}$ for an aperture radius of 5 μm and up to $q \approx 4\mu m^{-1}$ for the 10 μm one. Beyond these values the diffraction patterns cannot be detected adequately by the camera. The intensity slope differs systematically from theory, while the measured Airy pattern oscillation matches theory. Note that we measure the pinhole diffraction with unchanged LSP collection system. The slope discrepancy is likely caused by the incident beam influence given by the pinhole shape itself and the stray light of the BS.

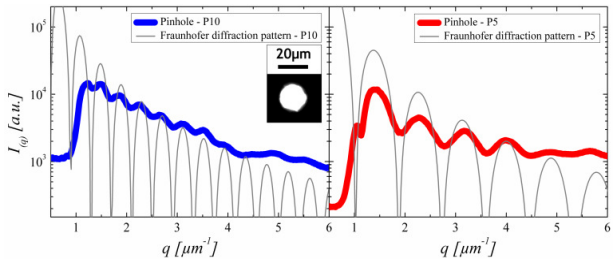

Fig. 5 Pinhole measurements for the calibration. The left figure shows P10 with an aperture radius of 10 μm, while P5 on the right has a radius of 5 μm. An image of the pinhole taken with an optical microscope is also shown.

The agreement between the measured LSP oscillations and the one theoretically predicted for both pinholes confirm the optical alignment of the system.

Results

To prove the capability of the SALS apparatus, different PSL particle sizes (reported in Table 1) have been measured. A comparison with the best matching theoretical Lorenz-Mie calculations confirmed the accuracy of our measurements in the entire meaningful q-range of $0.5 - 6.8\,\mu m^{-1}$. This wave-vector range shows a quantitative LSP oscillation from 1 up to 7 times for each measurement, giving the apparatus sufficient information to precisely characterize the measured particles.

Table 1 All particle sizes measured with the SALS apparatus are reported, where the prefix 'PSL', is used for polystyrene latex followed by the nominal diameter of the particle size. The refractive index values are reported for in-flow measurements only.

Particle	Nominal *[μm]*	Quiescent *[μm]*	In-flow *[μm]*	Refractive index
PSL 8	4.010 ± 0.049	4.000 ± 0.010	3.995 ± 0.025	1.588 ± 0.001
PSL 7*	N/A	N/A	3.433 ± 0.168	1.590 ± 0.001
PSL 6	3.042 ± 0.041	2.883 ± 0.006	2.859 ± 0.011	1.583 ± 0.002
PSL 5*	2.895 ± 0.088	2.807 ± 0.006	2.720 ± 0.198	1.586 ± 0.004
PSL 4	2.078 ± 0.031	2.020 ± 0.001	2.024 ± 0.009	1.587 ± 0.002
PSL 3*	1.644 ± 0.041	1.523 ± 0.006	1.530 ± 0.008	1.587 ± 0.003
PSL 2	0.947 ± 0.022	0.950 ± 0.001	0.929 ± 0.010	1.590 ± 0.016

* POLYSCIENCE particle

Note that the oscillation values are indicative for PSL particles and vary according to the composition of the measured particles. The more oscillations are present in a LSP, the more precisely the particle size and refractive index can be determined. Indeed, a variation of less than 5% of the particle radius significantly changes the oscillation of a LSP in the q-range of the SALS apparatus. Generally, the bigger a particle size, the more distinct the change. In addition, LSP changes significant according to small variations of refractive index. PSL 8 particles for instance, show a modification of the LSP slope for varying refractive index, while a change of the particle radius causes an absolute shift of the LSP bigger than q ≈ 4 μm^{-1}. For an easier observation of the LSPs, all measurements are plotted with linear scaled abscissa, while a logarithmic scale is preferred for the ordinate.

Quiescent measurements

The LSPs of PSL particles of different radii normalized to an exposure time (ET) of 1 ms with overlaid corresponding Lorenz-Mie theory are summarized in Fig. 6. The obtained average particle sizes are reported in Table 1 for three separate particle measurements for each size.

We observed a higher number of LSP oscillations with the increase in size of particles. For each size a matching theoretical curve was found and overlaid, where minima and maxima positions agree the most. Indeed, the oscillations of the theoretical curves agree very well. The measured PSL 8 profile shows seven minima and maxima for the given q-range, where all peak positions agree very well with the pre-calculated theory. It is expected that the height of the first measured scattering peak is less pronounced due to the stray light subtraction of the used BS. The PSL 8 particle radius obtained from the overlaid Lorenz-Mie curve shows a size difference of 0.010 μm (Table 1) compared to the particle supplier value, highlighting in this context the accuracy of our developed SALS apparatus. Due to polydispersity from multi-particle scattering, the absolute intensity of some scattering minima does not match the theoretical calculated values.

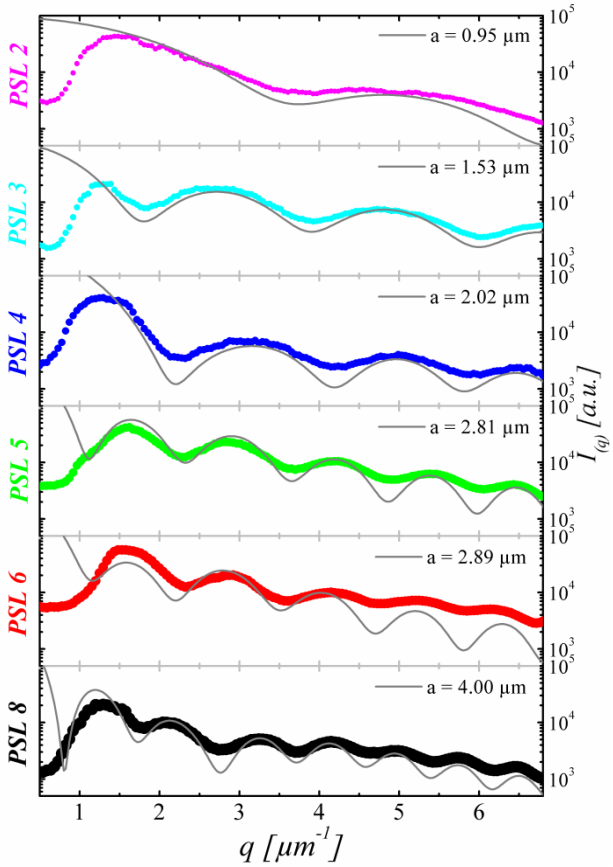

Fig. 6 Quiescent PSL measurements are plotted over the q-range of the apparatus. The corresponding Lorenz-Mie theory with radius a (indicated in legend of graphs) is overlaid in gray. One representative measurement curve for PSL 8, 6, 5, 4, 3 and 2 is shown for the respective particle size.

However, the theoretical calculated Lorenz-Mie LSP for the nominal PSL 6 particle value (not shown in Fig. 6) has an atypical low first scattering maximum ≈ 1.6 μm^{-1}, which is not returned in our measurement. Moreover, the PSL 6 LSP from 1 up to 3 μm^{-1} is highly sensitive to changes in particle radii. All other particles are characterized without difficulty over the whole q-range, where all measured peak heights correspond to theory. The correct measurement of the absolute scattering value for higher q-values is in general more challenging, due to the low scattering intensity and bigger influence of lens aberration. No optical vignetting effects were noticed during the measurements, since a small lens distance $p5$ was used, and multiple-element lenses at the scattered light collection system were avoided. All the measured particle sizes in quiescent conditions versus the nominal radii are summarized in Table 1.

Unsurprisingly, the PSL 6 measurement shows the most significant difference between measured and nominal radius. This result was expected, due to the more complex LSP and polydispersity for this particle size.

Refractive index measurements

LSPs of single particles can change significantly according to small variations in the particle refractive index or size. Note that the refractive index influences LSPs in a different way compared to changes caused by the particle radius (see Fig. 7).

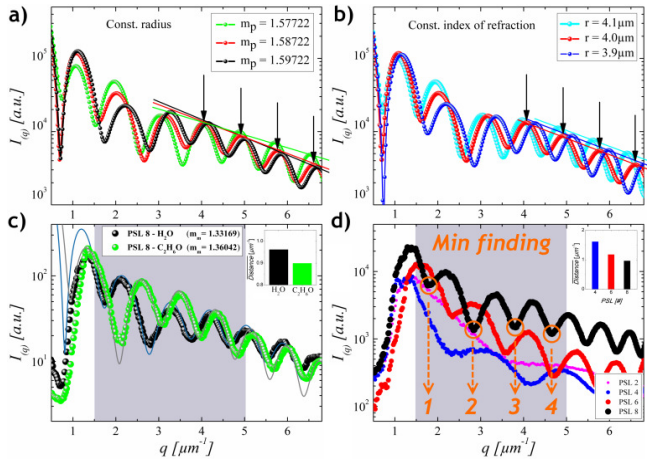

Fig. 7 The influence of the refractive index on the LSP is demonstrated on the example of PSL 8. a) Shows the change of slope at higher q-ranges for different particle refractive indices, while in b) the scattering slope change in the same q-range according to different particle radii is illustrated. c) A measurement with different refractive indices of the ambient medium is shown, where the solid line indicates the according theoretical LSP. The inset shows the average minima distance in the highlighted q-range for both measurements. d) The minima finding is illustrated, where the inset shows the averaged distance change over different measured particle sizes.

Therefore, an explicit distinction between radii and refractive index becomes possible. While a change of the particle refractive index (see Fig. 7a) displays a modification of the scattering profile slope, a change of the particle radius (see Fig. 7b) causes an absolute shift of the scattering profile at higher q-values. Fig. 7c illustrates a PSL 8 measurement with two different refractive indices of the medium, leading to a significantly different LSP result. Moreover, a significantly different average distance (see inset Fig. 7c) between LSP minima in the highlighted q-range (1.5 – 5 μm^{-1}) is recognized. This averaged minimum distance detection is implemented in our Matlab routine to restrict the input parameters for the Lorenz-Mie calculations. Fig. 7d illustrates the changing of the averaged minima distance in relation to the measured particle size, where the averaged LSP minima distance trend -for changing particle radius- is indicated in the inset. For the refractive index measurement -with our Matlab routine- each LSP peak in the highlighted range (for increasing q-values) is taken in consideration. These relative peak intensity values are compared with pre-calculated refractive index values. Indeed, by changing the restricted input parameters of the theoretical calculated Lorenz-Mie LSPs, a best-matching LSP can be found.

In-flow measurements

All previously measured PSL particles in quiescent conditions were subsequently analysed in-flow. In addition, a solution with all considered particle sizes mixed together was analysed to prove the multiplex ability of our apparatus. A minimum number of eight separate particle measurements was analysed for each particle size except for PSL 7, where three particle measurements were characterized. All particle scattering results are summarized in Fig. 8.

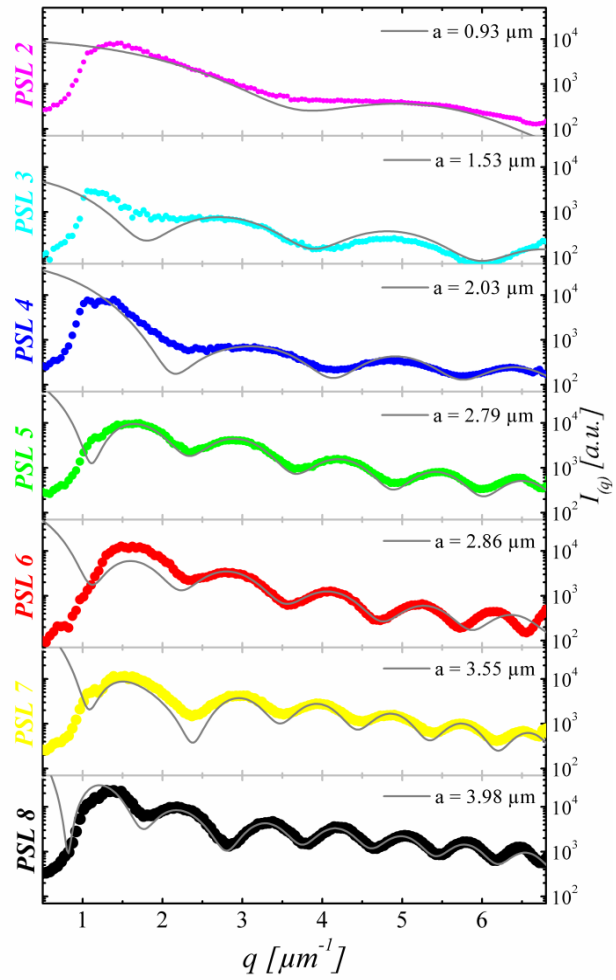

Fig. 8 One representative PSL particle measurement in-flow for each particle size is plotted over the q-range of the apparatus. All measured curves are normalized to an ET of 1 ms, while the corresponding Lorenz-Mie theory is overlaid in gray with radius a (indicated in legend of each graphs).

The LSPs of the particles match theory, where most scattering peaks are correctly measured in their position and height. The absolute intensity of the scattering minima was surprisingly well measured. Indeed, by excluding the first measured LSP minimum for each particle size, an almost perfect match between the measured LSP and theory was achieved. The first peak of each LSP illustrates a slight mismatching, caused by the BS presence. Note that small microfluidic misalignments of the particles can result in altered background noise values, effecting mainly q-values $< 2\ \mu m^{-1}$. At q-ranges bigger than $6\ \mu m^{-1}$, the measurements may show inaccuracy caused by

optical vignetting effects from the microfluidic device. The results highlight the opportunity to measure small variations in particle size or refractive index until q-ranges up to 6 μm^{-1}.
All measurements show consistent intensity patterns that linearly shift up with increase of ET.
Fig. 8 demonstrates also a particle size not listed by the particle supplier (Table 1). In fact, the particle size is the result of analysis from PSL 5 measurements. Due to the impurity of the solution from the supplier, two different particle sizes were detected in the stock solution. The amount of PSL 7 particle is very low compared to the amount of the main particle. The first minimum close to $q = 1\ \mu m^{-1}$ is not precisely detected, while the following minima match theory. For the proof of the PSL 7 existence in the PSL 5 solution, additional measurements with an inverted microscope (OLYMPUS - X81) were performed. These measurements clearly identified the existence of PSL 7 particles and justified the high polydispersity given from the particle supplier. For PSL 6 particles, our apparatus showed minor difficulties to correctly measure the LSP for q-values lower than 2.5 μm^{-1} and bigger than 5.5 μm^{-1}, while all other particle sizes matched well with theoretical predictions.
In addition, results from the real part of the particle refractive index -obtained by comparison with pre-calculated values- are shown in Table 1. The bigger a particle size, the more accurate the calculation of the refractive index.. Therefore, for PSL 2 measurements we can only identify a value range from 1.57 to 1.61. The reported refractive indices show very demonstrative the measuring ability of the apparatus.
In this context, the microfluidic measurements highlight the possibility to use this SALS apparatus for more sophisticated applications, where detecting and distinguishing micrometric particle sizes in continuous microfluidic flows is required. Moreover, we show that the apparatus measures particle in-flow very accurately, without loss of precision. Due to the measurement of individual particles improved by the 3D viscoelastic alignment, the LSPs are also more precisely recognized in terms of absolute minima intensities compared to quiescent measurements.

Multiplex measurements

Measurement of multi-particle solution in microfluidic flow is useful to understand the multiplex ability of the apparatus. Therefore, a solution mixed with all previously measured particle sizes was prepared. This solution was measured in the same conditions adopted for in-flow measurements. All particle sizes were separately recognized from the system over time, see Fig. 9(b). The corresponding theoretical predicted Lorenz-Mie LSPs are plotted in Fig. 9(a).
All curves were collected with constant ET. The absolute scattering intensity height of all curves -except PSL 2- matches theory. This implies that a PSL 8 particle scatters with a lesser intensity than a PSL 5 particle at a given q-value. The theoretical LSPs were calculated for constant incident laser power, while fluctuations of the incident light were possible during real measurements.

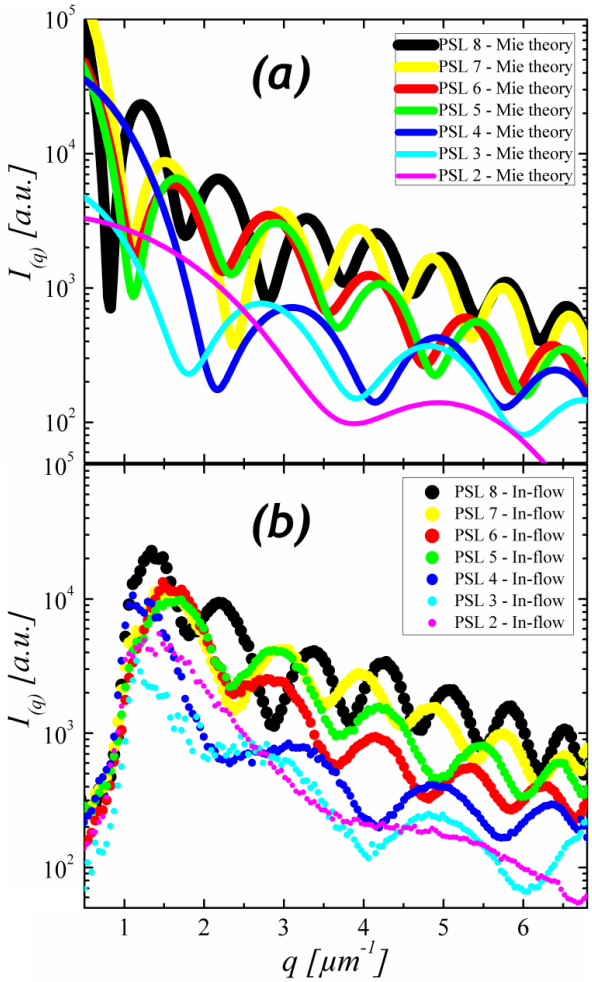

Fig. 9 (a) Theoretical Lorenz-Mie LSPs for all measured PSL particles. (b) In-flow results for a multi-particle measurement. Only one representative LSP for each particle size is shown. All measurements are collected with constant ET and incident laser intensity.

The absolute scattering intensity measured for PSL 2 particles differs from theory, according to possible multi-particle measurements. Due to constant pressure driven pumping of the particle solution through the microfluidic device during all our in-flow measurements, particle migration to the central axis of the channel appears less pronounced for particles smaller in diameter. Note that by changing the rheological or geometrical parameters of the viscoelastic particle alignment system, even smaller particle sizes can be aligned in the central axis according to the preferred particle range to be measured.
The SALS apparatus is built to measure up to 1.2 particle/s for the given ET and particle velocity. A throughput of 0.2 - 0.6 particles/s was chosen for the multiplex analyses to minimize multi-particle measurements. Note that the particle throughput can easy be regulated by the pressure pump.
The microfluidic multiplex measurements highlight the possibility to use our SALS system for applications where detecting and distinguishing micrometric particle sizes in continuous microfluidic flows is required.
We find agreement between the measured data and the nominal radii with discrepancies not higher than 7.3% in size and 1% in

refractive index. Thanks to the high sensitivity of the apparatus, particle size variations of less than 0.1 µm are detectable in microfluidic flows.

The precise particle size characterization -as well as the refractive index information from the measurement- opens up the possibility to use this apparatus in real multiplex applications. Compared to standard measurement techniques, a very low amount of target particle concentration is required for accurate results. The characterization of non-spherical -as well as non-rigid- particles[20] by an accurate obtained LSP is in general possible and therefore is worth considering for future applications.

Conclusions

We report a straightforward technique to measure morphological features of micrometric sized particles in microfluidic flows. A SALS system with a wide continuous LSP -combined with a precise particle alignment system induced by viscoelastic particle migration in-flow- has been optimised to measure particles ranging from 1 up to 4 µm in radius. The obtained optical layout of the apparatus allows the collection of LSPs ranging from 0.5 up to $6.8\,\mu m^{-1}$. Furthermore, the incident laser beam diameter and convergence over the given wide q-range for single particles are unique. Reliable results are obtained for both quiescent and in-flow measurements and match theoretical values. In comparison to holographic particle characterization systems, a comparable high morphological precision could be obtained in a cost-effective system, avoiding complex LSP calculations.

The reported particle alignment system, combined with the rectangular shaped microfluidic measuring chamber, can be easily implemented in other light scattering instruments, giving the possibility to analyse diverse LSPs of individual particle in microfluidic flows. In particular, cells of the human blood -range in the reported particle size of the apparatus- will be of interest, since the refractive index and radius is unknown or varies from cell to cell. We expect that this apparatus can be useful in improving the analysis of more complex particle shapes with different refractive indices and absorption coefficients.

Notes and references

[a] Center for Advanced Biomaterials for Healthcare@CRIB, Istituto Italiano di Tecnologia (IIT), Largo Barsanti e Matteucci 53, 80125 Naples, Italy.

[b] Interdisciplinary Research Centre on Biomaterials (CRIB), Università degli Studi di Napoli "Federico II", Piazzale Tecchio 80, 80125 Naples, Italy.

[c] Dipartimento di Ingegneria Chimica, dei Materiali e della Produzione Industriale, Università degli Studi di Napoli "Federico II", Piazzale Tecchio 80, 80125 Naples, Italy[b].

* E-mail: david.dannhauser@iit.it.

† On April 10th, 2013 our co-author, friend and colleague Giovanni Romeo suddenly died, aged 33. We all would like to dedicate this paper, to him. He will always stay with us and in our thoughts.

1 V.P. Maltsev, and K.A. Sem'yanov, Characterisation of bio-particles from light scattering, Walter de Gruyter, 2004.
2 F. Ferri, Rev. Sci. Instrum., 1997, **68**, 2265-2274.
3 M. Alexander, and F.R. Hallett, Appl. Opt., 1999, **38**(19), 4158-4163.
4 A. Wong, and P. Wiltzius, Rev. Sci. Instrum., 1993, **64**(9), 2547-2549.
5 L. Cipelletti, and D.A. Weitz, Rev. Sci. Instrum., 1999, **70**(8), 3214-3221.
6 E. Tamborini, and L. Cipelletti, Rev. Sci. Instrum., 2012, **83**(9), 093106-093106-8.
7 J. Neukammer, C. Gohlke, A. Höpe, T. Wessel, and H. Rinneberg, Appl. Opt., 2003, **42**(31), 6388-6397.
8 V.P. Maltsev, Russ. Chem. Bull., 1994, **43**, 1115-1124.
9 V.P. Maltsev, A.V. Chernyshev, K.A. Sem'yanov, and E. Soini, Appl. Opt., 1996, **35**, 3275-3280.
10 F.C. Cheong, B. Sun, R.U. Dreyfus, J. Amato-Grill, K. Xiao, L. Dixon, and D.G. Grier, Opt. Express, 2009, **17**, 13071-13079.
11 F.C. Cheong, K. Xiao, D.J. Pine, and D.G. Grier, Soft Matter, 2011, **7**, 6816-6819.
12 G. D'Avino, G. Romeo, M.M. Villone, F. Greco, P.A. Netti, and P.L. Maffettone, Lab Chip, 2012, **12**(9), 1638-1645.
13 D. Dannhauser, G. Romeo, F. Causa, and P.A. Netti, Proceedings of the International Conference on Optical Methods for Inspection, Characterization, and Imaging of Biomaterials, Munich, 2013.
14 G. Romeo, G. D'Avino, F. Greco, P.A. Netti, and P.L. Maffettone, Lab Chip, 2013, **13**, 2802-2807.
15 C.Mätzler, Matlab function for Mie scattering and absorption, IAP Res. Rep 8, 2002.
16 M. Bass and V.N. Mahajan, Handbook of Optics, Volume 1, McGraw-Hill, 3rd edn., 2010.
17 S.N. Kasarova, N.G. Sultanova, C.D. Ivanov, and I.D. Nikolov, Opt. Mater., 2007, **29**(11), 1481-1490.
18 G.M. Hale and M.R. Querry, Appl. Opt., 1973, **12**(3), 555-563.
19 C.F. Bohren and D.R. Huffman, Absorption and Scattering of Light by Small Particles, Wiley, 1983.
20 M.I. Mischenko, J.W. Hoenier, and L.D. Travis, Light Scattering by Nonspherical Particles: Theory, Measurements, and Applications, Academic Press Inc., 1999.

Table of content:

Colour graphic:

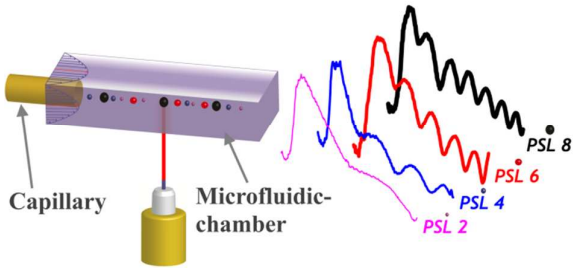

Text:

A method to combine precise particle alignment in-flow and light scattering profile characterization for micrometric sized particles is reported.